

This is the author's final, peer-reviewed manuscript as accepted for publication (AAM). The version presented here may differ from the published version, or version of record, available through the publisher's website. This version does not track changes, errata, or withdrawals on the publisher's site.

Influence of charge transfer on the isomerisation of stilbene derivatives for application in cancer therapy

Nicole Holzmann, Leonardo Bernasconi, Roger H. Bisby
and Anthony W. Parker

Published version information

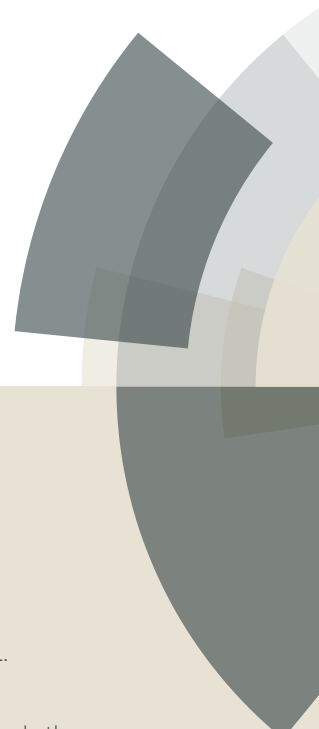
Citation: N Holzmann et al. "Influence of charge transfer on the isomerisation of stilbene derivatives for application in cancer therapy." *Physical Chemistry Chemical Physics*, vol. 20, no. 44 (2018): 27778-27790.

DOI: [10.1039/C8CP05375H](https://doi.org/10.1039/C8CP05375H)

This version is made available in accordance with publisher policies. Please cite only the published version using the reference above. This is the citation assigned by the publisher at the time of issuing the AAM. Please check the publisher's website for any updates.

PCCP

Accepted Manuscript



This article can be cited before page numbers have been issued, to do this please use: N. Holzmann, L. Bernasconi, R. H. Bisby and A. W. Parker, *Phys. Chem. Chem. Phys.*, 2018, DOI: 10.1039/C8CP05375H.



This is an Accepted Manuscript, which has been through the Royal Society of Chemistry peer review process and has been accepted for publication.

Accepted Manuscripts are published online shortly after acceptance, before technical editing, formatting and proof reading. Using this free service, authors can make their results available to the community, in citable form, before we publish the edited article. We will replace this Accepted Manuscript with the edited and formatted Advance Article as soon as it is available.

You can find more information about Accepted Manuscripts in the [author guidelines](#).

Please note that technical editing may introduce minor changes to the text and/or graphics, which may alter content. The journal's standard [Terms & Conditions](#) and the ethical guidelines, outlined in our [author and reviewer resource centre](#), still apply. In no event shall the Royal Society of Chemistry be held responsible for any errors or omissions in this Accepted Manuscript or any consequences arising from the use of any information it contains.

Influence of Charge Transfer on the Isomerisation of Stilbene Derivatives for Application in Cancer Therapy

Nicole Holzmann¹, Leonardo Bernasconi¹, Roger H. Bisby², Anthony W. Parker¹

¹STFC Rutherford Appleton Laboratory, Harwell Oxford, Didcot OX11 0QX, UK

²School of Environment and Life Sciences, University of Salford, Salford M5 4WT, UK

Abstract

The photoisomerisation of non-toxic *trans*-combretastatin CA4 to its cytotoxic *cis* isomer demonstrates the high potential of this and similar compounds for localised cancer therapy. The introduction of intramolecular charge-transfer character by altering the substituents of combretastatin systems opens up possibilities to tailor these stilbene derivatives to the special demands of anticancer drugs. In this TDDFT study we explore how absorption wavelengths for both the *trans* and *cis* isomers can be red shifted to enable deeper light penetration into tissue and how the *trans*→*cis* and *cis*→*trans* isomerisation are affected by charge transfer effects to different degrees.

Introduction

Photodynamic Therapy (PDT) has several advantages compared to chemotherapeutic cancer treatment [1]. In particular, the advantages of PDT are its ability to target cancer at a very specific and localised level via the precise activation by illumination of photosensitising drugs directly in the vicinity of malignant cells, while healthy (but similar) cells throughout the patient's body are unaffected by inactive drug molecules [2]. Most PDT drugs rely on photosensitizing the generation of cell damaging singlet oxygen induced by photoexcitation of the drug at the tumour site. Recently new PDT drugs that are not limited to cell destruction by singlet oxygen have also been developed, including Combretastatin A4 (CA4), first isolated by Pettit [3], which effectively disrupts tubulin polymerisation and thus the formation of tumoral vasculature [4]. However, this drug is not usable for clinical applications because of its severe side effects [5,6]. Combretastatins are functionalised stilbene derivatives and therefore exist in two isomeric forms, *cis* and *trans*. It is *cis*-CA4 that is cytotoxic, and this species can be generated by photoisomerisation of the *trans*-CA4 [7], which is considerably less toxic [8-11]. We previously reported that the usual one-photon excitation wavelength of the latter is around 340 nm [12], which is too short for physiological use, because tissue absorption below 400 nm is high. On the other hand, longer and readily tissue-penetrating wavelengths in the red or near-infrared region (600-900 nm) can be achieved by two- or three-photon excitation (2/3PE) of *trans*-CA4 [13], which, however, suffers from reduced absorption cross sections [14,15]. One potential strategy to overcome this issue is to develop combretastatins that possess intramolecular charge-transfer character through the addition of an electron donor group and an electron acceptor group respectively on each of the phenyl rings, to produce not only a higher multiphoton absorption cross section, but also a redshift in the absorption and fluorescence spectra, promoting light tissue penetration [16].

As a further step in the search of tuneable photo-isomerisable drug candidates, we recently have conducted a theoretical study on *trans* combretastatins and stilbene derivatives of different intramolecular charge transfer extent [17]. Consistent with our experimental results, we were able to confirm that the absorption wavelength redshifts and the oscillator strength increase for molecules with larger charge-transfer character. Similar to the well-known photoisomerisation process of stilbene [18-20], one electron from the HOMO (with π bonding character with respect to

the vinyl C=C bond) is excited to the respective anti-bonding LUMO, reducing the C=C bond order and facilitating bond rotation in all combretastatins. However, we observed that the elongation of the central C=C bond on excitation was slightly larger for derivatives of low charge-transfer character, while the relaxation energies for the fluorescence from the S_1 surface to the ground state were higher. Under the assumption that the barrier for rotation around the central C=C bond on the S_1 surface is similar to the widely studied barrier in stilbene, these are indicators that a reaction barrier might be overcome more readily than in combretastatins of higher charge-transfer character. However, with a shift of charge throughout the molecule, the potential energy surfaces (PESs) might differ from the symmetrical stilbene one, not only in barrier heights, but also in the existence and location of a conical intersection. Changes in the symmetric stilbene isomerisation PES can lead to an unequal *cis/trans* probability in the isomerisation from the excited state. To examine the effect of substituent groups on the PES topology, we present here a study of the ground and S_1 PES of four stilbene derivatives with different charge-transfer characters.

The introduction of electron pushing and pulling groups can also have other consequences. The molecule DMABN (4-(N,N-dimethylamino)benzonitrile) is an archetypical charge-transfer system, which consists of an electron pulling nitrile group and an electron pushing dimethylamino group in *para* position on a single benzene ring. DMABN is planar in its ground state, but in its excited S_1 state it can undergo a twist of the amino group with respect to the phenyl ring. Although theoretical studies indicate variations between 45 and 90° (depending on the applied method and the pyramidal angle) for the twist angle that locally separates the charges in this molecule, they all confirm it to be a local minimum structure on the S_1 surface [21-24]. Fluorescence from this twisted intramolecular charge-transfer (TICT) state occurs at lower energies than in the planar locally excited (LE) state, which leads to the experimentally observed dual fluorescence of DMABN [25,26]. *Trans*-stilbene has been described in experimental and theoretical studies as being approximately planar in its crystal phase [27,28], but with a shallow potential energy profile for the rotation of the phenyl rings around the C–C single bonds in both ground [29] and excited [30] state. Owing to the symmetry of this molecule, there is no charge separation, and a TICT state cannot therefore appear in competition with the photoisomerisation pathway in *trans*-stilbene through the phenyl ring rotation. Functionalised charge transfer stilbenes, like 4-dimethylamino-4'-cyanostilbene (DCS), have been studied with experimental

and theoretical methods for more than forty years, but there is no general consent concerning the existence and nature of the TICT state. The dual fluorescence phenomenon of DCS can be partially explained by the existence of a TICT state formed by rotation around the C–C anilino bond [31-33] or the C–N amino bond [34-37], but no evidence for the existence of a TICT state and/or of dual fluorescence has been found in several studies [38-40]. Excited state re-absorption of fluorescence has been proposed as a potential alternative to the formation of a TICT state [41]. The formation of a TICT state was observed in experiments carried out at high temperature in polar solvents, and it was assigned to the S_1 surface. Rotation of the electron pulling phenyl ring has been described for other charge-transfer stilbenes, like 4-dimethylamino-4'-nitrostilbene [42].

In this study, we present and explore the different possible molecular rearrangement pathways on the S_1 surface for anticancer drug candidates with different substituent groups. We also address briefly the issue of the TICT state existence, although we remark that a proper study of this particular state would require an extensive analysis of solvent and temperature effects, which are beyond the scope of this work.

Methods

Theoretical calculations were carried out using the NWChem6.6 program package [43]. Ground state optimised structures were obtained using density-functional theory (DFT) at the B3LYP [44,45]/def2-TZVPP [46] level of theory. Stationary points were characterized as minima by calculating the Hessian matrix analytically. For vertical excitations and excited state optimisations the TDDFT method [47] was applied with the long-range corrected CAM-B3LYP [48] functional and kernel, which is known to typically yield accurate charge transfer excitation energies in molecular systems [49,50] and from which we obtained good qualitative agreement with experimental UV/VIS absorption and fluorescence spectra in our previous studies [17]. Absorption and fluorescence spectra were calculated considering the 50 lowest singlet excited states. For comparison, additional geometry optimisations of the ground state molecules were also carried out with the CAM-B3LYP functional. Scans were carried out using stepwise rotations of the dihedral angle of the central C=C double bond or its adjacent C–C single bonds in steps of 10°, 5° or 2°. Single point calculations of ground and first excited states were carried out at the CAM-B3LYP/def2-TZVPP level.

Deformation densities and charge transfer properties were obtained by subtracting the excited state and ground state densities [51,52], using single-point calculations on the ground state geometries using the Gaussian09 [53] program suite. The same approach was used to calculate atomic partial charges and Wiberg Bond Orders (WBOs) [54] at the CAM-B3LYP/def2-SVP level with the NBO 6.0 (Natural Bond Orbital) method of Weinhold et al. [55].

The ‘COnductor-like Screening MOdel’ (COSMO), as implemented in Gaussian09 [56,57], was used to describe the effect of seven different solvents at $T = 20\text{ }^{\circ}\text{C}$ [58].

Results and Discussion

According to our previously published results on *trans*-combretastatins, our *cis* test set consists of two combretastatins with small charge-transfer character, namely CA4 (**1c**) and the fluorinated compound CA4F (**2c**), and two other stilbene derivatives **3c** and **4c** (Scheme 1), which exhibit considerable charge-transfer effects in the excitation to the S_1 state for the planar *trans* analogues. In **3c** (CA4CN), the charge-transfer character is introduced via the addition of a nitrile group in *para* position on the aromatic ring **II**, opposing the electron pushing methoxy groups in *para* and *meta* position of ring **I**. 4-amino-4'-cyano stilbene (ACS, **4c**), on the other hand, has only one electron pushing amino group in *para* position of ring **I**. The corresponding *trans* analogues will be referred to as **1t** to **4t**.

1. Optimised Structures, Charge Transfer, Absorption and Fluorescence Spectra

Geometry optimisations on all *cis* systems were carried out for the gas phase ground state (S_0 , DFT) structures at the B3LYP/def2-TZVPP and CAM-B3LYP/def2-TZVPP levels, and the first excited state (S_1 , TDDFT) at the CAM-B3LYP/def2-TZVPP level. Selected distances (d_A , d_B and d_C) and dihedral angles (θ_A , θ_B and θ_C) for the C=C (B) and C-C (A, C) vinyl bonds are given in Table 1. The overall agreement between the ground state structures calculated with B3LYP and the long-range corrected functional CAM-B3LYP are in general good, with a deviation of 0.011 Å for the central C=C double bond and slightly more acute dihedral angles for the latter functional for all *cis* compounds. Comparison of the structure of **1c** with its experimental crystal structure [59] shows only significant differences of over 20° for the dihedral angle θ_A , which can be caused by the existence of a different local minimum on the shallow potential energy surface for the rotation of one of the flexible methoxy groups linked to **I**. Our calculated values lie within the range of previously reported data on *cis*-stilbene for the C=C double bond in the ground state ($d_B(\text{CASSCF}) = 1.327 \text{ \AA}$ [30], $d_B(\text{B3LYP}) = 1.352 \text{ \AA}$ [60] and $d_B(\text{MP2}) = 1.356 \text{ \AA}$ [61]), but they are in all cases slightly shorter for the C-C single bonds ($d_{A/C}(\text{CASSCF}) = 1.486 \text{ \AA}$, $d_{A/C}(\text{B3LYP}) = 1.477 \text{ \AA}$ and $d_{A/C}(\text{MP2}) = 1.478 \text{ \AA}$). For the excited-state TDDFT calculations of *cis*-stilbene, the C=C bond B length corresponds to that observed for the non-charge transfer compounds **1c** and **2c** ($d_B(\text{PBE0}) = 1.417 \text{ \AA}$), while bonds A and C

are longer ($d_{A/C}(\text{PBE0}) = 1.412 \text{ \AA}$) [62]. As for the *trans*-combretastatins, excitation to the S_1 surface occurs by promotion of one electron of the HOMO to the LUMO (Figure 1 for **3t** and **3c**). While the HOMO exhibits π bonding character for the central bond B and π^* anti-bonding character for bonds A and C, the situation is reversed for the LUMO. As a consequence, we observe bond elongation for bond B and a shortening of bonds A and C after excitation. As we have described for the *trans* isomers [17], the bond lengths of the central bond B elongates to less for the charge-transfer compounds **3c** ($d_B = 1.409 \text{ \AA}$) and **4c** ($d_B = 1.408 \text{ \AA}$), in comparison to S_1 bond lengths of B in the non-charge transfer combretastatins **1c** ($d_B = 1.417 \text{ \AA}$) and **2c** ($d_B = 1.416 \text{ \AA}$) and the reported distances for (non-charge transfer) *cis*-stilbene ($d_B(\text{PBE0}) = 1.417 \text{ \AA}$) are longer. However, the absolute bond distances for B are larger for the *cis* isomers, which also results in a larger absolute elongation. The overall bond length changes are $\Delta d_{B(S_1-S_0)}(\mathbf{1}) \approx \Delta d_{B(S_1-S_0)}(\mathbf{2}) > \Delta d_{B(S_1-S_0)}(\mathbf{3}) > \Delta d_{B(S_1-S_0)}(\mathbf{4})$. More pronounced structural changes after excitation can be observed in the dihedral angles. While in the ground-state *trans*-stilbene derivatives the single bonds A and C are close to planarity, in the *cis* isomers planarity cannot be achieved because of the steric repulsion, which results in dihedral angles $\theta_{A/C}$ between 140 and 155°. It has recently been shown that for very bulky substituents like *tert*-butyl groups attached to the meta positions of the phenyl London dispersion interactions can play an important role while they are negligible in unsubstituted *cis* stilbene [63]. Populating the LUMO, thereby increasing the double bond character in bond A and C, leads to a significant increase in the dihedral angles $\theta_{A/C}$: 167.7° for θ_C in **4c** to 172.7° in **2c**. Overall the non-charge transfer compounds are therefore closer to planarity. Compensating for the steric repulsion, bond B (accounting for less than 10° in all studied ground-state structures) rotates by 39.1 and 38.1° for the non-charge transfer combretastatins **1c** and **2c** and 30.9 and 30.7° for **3c** and **4c** in the relaxed S_1 state. Interestingly, in this state the dihedral angles of the charge-transfer compounds for the bonds θ_C are smaller (2.0° for **3c** and 4.2° for **4c**) than their counterpart θ_A . In contrast to **3t** and **4t**, where π electrons can move along the planar and fully conjugated entirety of the molecule, the movement of π electrons is restricted in the *cis* isomers. While bond A has access to the π electrons of the aromatic ring **I** with its electron donating substituents pushing electron density towards bond A, bond C is not affected, because of its non-planar geometry. Furthermore, this bond experiences the electron depletion effect caused by the electron-pulling group in the *para* position of ring **II**. In summary, increasing the charge-transfer character in stilbene derivatives, which has shown to

be beneficial for the planarity in both ground and first excited state of the *trans* isomers, has the opposite effect in the ground and excited states of the *cis* conformations.

The charge-transfer character in all *cis* compounds was quantified in their ground state geometries by subtracting their ground state electron density from the S_1 electron density. The corresponding charge-transfer deformation densities $\Delta\rho_{(S_1-S_0)}$ are shown in Figure 2 and numerical values are given in Table 2, along with results obtained from our previous work. This analysis confirms similar and small charge transfers for combretastatins **1c** and **2c**, while the charge-transfer dipole amounts to 5.7 D for **3c** and 7.2 D for **4c**. Both the amount of transferred charge and the charge-transfer dipole are larger in the *cis* isomers. This finding is not trivial as the ability of the π electrons to freely move along the planar conjugated system in *trans* stilbene derivatives would suggest the greatest possible transfer of charge to occur in the *trans* isomers rather than in the *cis* compounds where a breakup of molecular planarity should also inhibit electron flow. Similar to the described TICT state in DMABN [25,26], the spatial separation of charge in the *cis* isomer leads to a separation of charge by reducing the communication between the donor and acceptor parts of the molecule. We observe (Figure 2) that, the areas of charge depletion (red) and charge accumulation (blue), especially in the central region of the molecules, are more asymmetrical in the charge-transfer isomers, e.g. the depletion lobe of the central bond B in **3c** and **4c** clearly shows an extension towards the atoms of bond C. This is caused by two factors. A comparison of the orbital shapes of the HOMO and LUMO of the stereoisomers (see Figure 1 for **3**) shows that even for the charge-transfer compound **3t**, HOMO and LUMO have a rather uniform distribution along the central C=C bond in the HOMO and at the participating vinyl carbon atoms in the LUMO, whereas in **3c** the frontier orbitals have a more localised distribution of electrons at the two central atoms and thus a better separation of charge, owing to the twisted geometry. Secondly, the calculated absorption spectra of the *trans* compounds indicate that the main and only dominant peak is assigned to the HOMO→LUMO transition, and therefore the total charge-transfer deformation density mirrors the rather uniform HOMO and LUMO distribution. The calculated absorption spectra of **1c** to **4c** are shown in Figure 3 (left, for complete data see Supporting Material Table S1–S4). The peaks above 280 nm correspond to the HOMO→LUMO transition and red shift with increasing charge-transfer character. Other peaks of lower, but still significant intensity can be found e.g. in the areas around 180, 190 and 225 nm. These peaks mainly correspond to different transitions HOMO-1, HOMO-2 and HOMO-3 to

LUMO+1, LUMO+2 and LUMO+3. These orbitals are shown for **1c** to **4c** in the Supporting Information Figure S1–S4. They are largely localised on one of the aromatic rings and contribute to the change of total electron density in the excited state.

Calculated CAM-B3LYP/def2-TZVPP absorption and fluorescence spectra at the HOMO→LUMO transition peak for the *cis* and *trans* isomers of **1** to **4** in gas phase are shown in Figure 3 (right) and Table 3. The absorption corresponds to the vertical excitation from the S_0 ground state to the S_1 excited state surface for the calculated ground state structures. Fluorescence corresponds to the de-excitation to S_0 after geometry optimisation in the S_1 state. Absorption in the *cis* derivatives occurs at slightly lower wavelengths than in the *trans* analogues (between 295 nm for **1c** and 326 nm for **4c**), but the trend in the red shift of the absorption with increased charge-transfer character is well reproduced, with the two non-charge transfer compound excitation energies only differing by 3 nm. After excitation, the *cis* isomers undergo considerable geometrical changes during the relaxation on the S_1 surface, and the fluorescence peaks are therefore located at lower energy (ca. 490 nm). Interestingly, the fluorescence charge-transfer dependent red shift of the *cis* isomers is reversed. The Stoke's shift of these molecules therefore follows the trend $\nu_{A-F}(\mathbf{1}) \approx \nu_{A-F}(\mathbf{2}) > \nu_{A-F}(\mathbf{3}) > \nu_{A-F}(\mathbf{4})$, which clearly indicate dependence on the extent of intramolecular charge transfer on promotion to S_1 . Oscillator strengths [64] for absorption and fluorescence (**1c**: 0.54/0.35, **2c**: 0.48/0.34, **3c**: 0.48/0.32 and **4c**: 0.53/0.40) are substantially lower than in the *trans* isomers and do not show any correspondence to the charge transfer properties of the *cis* compounds.

2. S_0 and S_1 potential energy surfaces

The determination of the potential energy surfaces of the ground S_0 and the electronically excited S_1 state was carried out as a sequence of single-point and vertical excitation energy calculations at the CAM-B3LYP/def2-TZVPP level, by rotating the central C=C bond (B) in 10° steps between 140° and -40° . For the stilbene derivatives, the existence of a shallow minimum in the PES for the rotation around the two C–C single bonds A and C has been reported [29]. As the steric repulsion has a strong effect on the total energies, we used the ground state of the *cis* structures **1c** to **4c** (where the aromatic rings are most twisted, allowing the C=C dihedral angle

to be small) as starting and reference points. The calculated PES are shown in Figure 4, in which the relative positions of the ground and excited state optimised structures (rectangles) and their energies from vertical excitation/de-excitation (circles) are also indicated.

The energy curves for the rotation of **1-4** in the ground state nearly perfectly overlap with each other. Only at the maximum (corresponding to a twisting angle of -90°) a minor deviation (3.1 kcal/mol) between the compound with the lowest (**1**) and highest (**4**) charge-transfer character is observed. The deviation in energy of the optimised ground state *trans* structures from the scan is satisfactorily minor, with difference of at most 3.3 kcal/mol at 180° . A lower energy is of course expected for the optimised structures, but this small deviation confirms that the rotation of bonds A and C, which are kept fixed at the values of the *cis* structures in the scan, has only a minor influence on the total energy. Also, the vertical de-excitation energies for the optimised *trans* S_1 structures lie less than 6 kcal/mol above the ground state scan at 180° .

After excitation, once the intramolecular charge shift takes place, a separation of the S_1 potential energy curves is observed, which is caused by the different charge-transfer character of the four molecules. This separation is less well defined in the area of the conical intersection ($\theta_B = -90^\circ$), but it is evident in the vicinity of the vertical excitation geometry on both the *trans* and *cis* side. As observed in the calculated absorption spectra, a lower amount of energy is required to excite the molecules with higher charge-transfer character, and the S_1 surfaces of **3** and **4** therefore lie below those of **1** and **2**. However, more important for anticancer drug application is the reaction barrier of the *trans*→*cis* isomerisation, thus the rotation barrier of bond B towards the conical intersection at $\theta_B = -90^\circ$. The energy of the S_1 surface seem to be noticeably influenced by the rotations around the bonds A and C, as the optimised S_1 *trans* and *cis* structures and the vertically excited *trans* ground-state structure are considerably lower in energy than the structures used in the scan (diamonds in Figure 4). Also, the optimised local minimum on the *cis* side of the S_1 surface appears to be located at a significantly larger rotational angle for B (around -40°), whereas, in the scan, the most stable structure for all molecules is at $\theta_B = -10^\circ$. Furthermore, the reversed fluorescence redshift of the *cis* compounds relative to the *trans* analogues indicates that the relative height of the S_1 PES for the four studied molecules can also be reversed in this area of the *cis* rotation coordinate, and therefore that it can differ from the PES obtained in the scan. As the energetic barriers on the S_1 surface obtained from the scan are

relatively small (less than 10 kcal/mol), the energetic contribution of the rotations around bonds A and C can affect the results. Taking this into account, we carried out additional single-point calculations using the excited (*trans* and *cis*) state optimised structures as starting points and scanning along the C=C bond B coordinate towards the reaction barrier in rotations steps of 10° (far from the barrier) and 5° (near the barrier) (see Supporting Information Figure S5). Direct comparison of the barriers of the *trans*→*cis* and the *cis*→*trans* isomerisation from the scan reveals that the latter is energetically slightly favoured only for the non-charge transfer compounds (1.2 kcal/mol for **1** and 1.0 kcal/mol for **2**). This finding is consistent with the models for the isomerisation of stilbene, in which the *cis*→*trans* isomerisation has been described as either barrierless or nearly barrierless, while the *trans*→*cis* isomerisation clearly shows an energetic barrier [18,62]. The difference in barrier heights for the *cis*→*trans* isomerisation with respect to the *trans*→*cis* isomerisation appears to vanish when charge transfer character is introduced in the system, as the isomerisation barriers have the same ($\Delta E_{(t \rightarrow c)-(c \rightarrow t)} = 0.0$ kcal/mol for **3**) or nearly the same ($\Delta E_{(t \rightarrow c)-(c \rightarrow t)} = -0.2$ kcal/mol for **4**) height. Our results suggest that the relative barrier heights for the *trans*→*cis* and the *cis*→*trans* isomerisation can be reversed via the introduction of charge-transfer character in the excitation to the S₁ state. It should be noted that our results are not sufficiently accurate to conclusively prove this point, and other more accurate methods for excited states may be required. However, we can confirm on the basis of our calculations that the energetic gap between the two isomerisation directions is more pronounced in the non-charge transfer molecules. For the isomerisation from the *trans* to the *cis* conformation of relevance to the anticancer properties of the species examined here, this indicates that molecules residing on the S₁ surface in *cis* conformation (either from skipping the conical intersection to S₁ minimum structure on the *cis* side of the PES or from re-excitation of *cis* conformers from the S₀ state) are more likely to isomerise back to *trans* for compounds with low charge-transfer character. On the other hand, the *trans*→*cis* isomerisation process shows overall lower barriers for the non-charge transfer compounds ($\Delta E_{(t \rightarrow c)}(\mathbf{1}) = 4.0$ kcal/mol and $\Delta E_{(t \rightarrow c)}(\mathbf{2}) = 4.4$ kcal/mol) than for large charge-transfer ones ($\Delta E_{(t \rightarrow c)}(\mathbf{3}) = 5.8$ kcal/mol and $\Delta E_{(t \rightarrow c)}(\mathbf{4}) = 5.4$ kcal/mol). Non-charge transfer stilbene derivatives therefore isomerise more readily than their charge-transfer analogues. It should be noted that not only the energetic differences between the different processes for the studied compounds are very small, but also all of the calculated barriers are below 10 kcal/mol. Kinetic rates and whether the reactions occur

spontaneously at body temperature can only be determined with certainty by calculating Gibbs free energies of optimised local minima and transition state structures in the S_1 state. Experimentally, combretastatins **1t** and **2t** photoisomerise at room temperature [12,14,16], and we therefore expect a similarly efficient photoisomerisation in the case of the charge-transfer derivatives at body temperature.

From the scan of our stilbene derivatives, we observe that the energetic maximum on the S_0 surface and the energetic minimum on the S_1 surface are at $\theta_B = -90^\circ$. The corresponding structures do not represent the exact structures at the conical intersection, but are expected to be reasonably close. TDDFT, which uses a single-reference wave function ansatz does not accurately describe conical intersections [65] and near-degenerate states [66]. However, the energetic gap at the S_0/S_1 conical intersection for SA-2-CAS(2/2) pre-optimised stilbene is satisfactorily described with TDDFT, with $\Delta E_{(S_1-S_0)} = 5.8$ kcal/mol for B3LYP/6-31G and $\Delta E_{(S_1-S_0)} = 0.7$ kcal/mol for B3LYP/6-31G** single-point calculations. Furthermore, in this pre-optimised conical intersection structure, a pyramidalisation angle $\tau = 32^\circ$ at the C=C carbon atoms was observed, while the S_1 PES was found to be very shallow for the pyramidalisation coordinate [67]. Similarly, but a saddle point on the S_1 surface is twisted ($\theta = 90^\circ$) ethylene. Furthermore, it does not have a detectable pyramidalisation barrier [68]. The energy gaps $\Delta E_{(S_1-S_0)}$ at $\theta_B = -90^\circ$ for non-optimised **1-4** with CAM-B3LYP/def2-TZVPP range from 4.4 kcal/mol (**1**) to 6.0 kcal/mol (**4**). They are only slightly higher than the stilbene gap computed at the B3LYP/6-31G** level (0.7 kcal/mol) [67], which can be attributed to minor energetic contributions from the pyramidalisation of the C=C bond carbon atoms, the fixed dihedral angles of bonds A/C and the phenyl substituents that were not optimised at $\theta_B = -90^\circ$. The altered electronic distribution in the charge-transfer derivatives is likely to have an influence on the location of the conical intersection for the C=C rotation coordinate and, more importantly, on the existence of the conical intersection itself, and therefore on the relative distance of the S_0 maximum and the S_1 minimum along the reaction coordinate. For anticancer activity, it is more favourable to have the S_1 minimum located at a larger distance from the S_0 maximum along the *cis* coordinate, as this increases the isomerisation yield. In order to obtain this information about the conical intersection we carried out additional scanning steps in the vicinity of the conical intersection with a reduced step size of 2° in both directions, namely at $\theta_B = -92^\circ$ and $\theta_B = -88^\circ$. To maintain the energetic deviation caused by the phenyl rotation low and to obtain reliable

results, we carried out these calculations with both the ground state *trans* and the ground state *cis* structures as reference structures, hence maintaining all structural features (including the phenyl ring rotation) unchanged, and only adjusting the C=C rotational angle θ_B (for full data see Supporting Information Table S7). In all calculations we found that the conformation with the highest energy on the S_0 surface to also have the lowest energy on the S_1 surface. This means that the conical intersection is conserved, and no relative shift of its extrema takes place. Therefore, the *cis/trans* 50/50 isomerisation ratio after de-excitation can neither be enhanced nor impaired by modifying the charge-transfer character of the molecule. When determining the location of the conical intersection on the C=C rotational coordinate it is most useful to analyse the approach direction from the *trans* side ($\theta_B = -92^\circ$), with the results obtained from the *trans* ground state reference structure and the approach from the *cis* side ($\theta_B = -88^\circ$) from the *cis* ground state reference structure accordingly, to avoid the comparatively large errors in energy caused by the lack of relaxation of the molecule periphery. We observe that, approaching the conical intersection both from the *trans* and from the *cis* side, an alteration of the rotational angle θ_B by 2° decreases the energy of the S_0 surface ($\Delta E_{(90^\circ-92^\circ)}$ between 2.8 and 3.0 kcal/mol and $\Delta E_{(90^\circ-88^\circ)}$ between 3.4 and 3.6 kcal/mol) while on the S_1 surface the energy increases ($\Delta E_{(90^\circ-92^\circ)}$ between -4.4 and -5.9 kcal/mol and $\Delta E_{(90^\circ-88^\circ)}$ between -4.4 and -5.6 kcal/mol). No influence from the charge-transfer substituents could be detected. We therefore conclude that, in all cases, the conical intersection is located at -90° , in analogy to stilbene, and, as we have shown in Figure 4, that the introduction of charge-transfer substituents does not play a significant role.

3. Exploration of S_1 surface for stable alternative conformations

As for the charge-transfer molecule DMABN, the charge-transfer stilbene derivatives **3t** and **4t** may undergo structural changes alternative to the rotation of the C=C central double bond, as a competing pathway to the isomerisation on the S_1 surface. This can lead to a structure with a characteristic charge separation. Formation of such an alternative stable conformation (corresponding to a TICT state in DMABN) could potentially decrease the isomerisation yield or even prevent the isomerisation altogether, impacting the application of the drugs in local cancer therapy. We have shown that the experimentally observed main fluorescence peaks agree well with the calculated fluorescence from relaxation without major peripheral structure changes.

Nevertheless, a competitively formed twisted conformation could theoretically fluoresce in the same region. In order to exclude this possibility, we carried out scans with a 10° step size between 80 and -170° for the two mainly discussed TICT coordinates for charge-transfer stilbenes: rotation around bond A that connects the electron donating phenyl ring to the central C=C bond [31-33] and around bond C for the electron accepting phenyl ring [42]. The results are displayed in Figure 5 for the S_1 surface for the non-charge transfer combretastatin **1t** and its charge-transfer analogue **3t**. In all cases, a monotonic increase in energy from the minimum at 180° to the maximum at 90° is observed. The energy required to reach the maximum amounts to more than 25 kcal/mol, which is significantly higher than both the *trans* and the *cis* isomerisation barriers. We therefore conclude that no stable twisted state is formed by rotation around bonds A and C in preference to the isomerisation process. Furthermore, the rotation of the methoxy group in *para* position or a simultaneous rotation around A and C of **3** do not result in an energetic minimum (see Supporting Information Figure S6 and S7).

4. Solvent Influence on Charge Transfer Character

We recently studied the experimental and calculated fluorescence red shifts in the spectra of the charge-transfer compounds **3t** and **4t** for polar solvents [17]. With the aim of tailoring charge-transfer stilbene combretastatins for cancer therapy, it is important to assess the influence of the solvent polarity on the charge-transfer character of these molecules, particularly since the anticancer activity must occur in physiological conditions, i.e. in the presence of water, although our previous imaging work indicates that both isomers of combretastatins **1** and **3** tend to concentrate in lipid droplets and are expected to interact with the tubulin target after diffusion of an equilibrium concentration within the aqueous cytoplasm [69,16]. Our time-resolved infrared (TRIR) and fluorescence lifetime experiments furthermore suggest that the solvent polarity in cells is similar to that of ethylene glycol, the microviscosity of the hydrophobic interiors of lipid bilayer membranes (0.5 and 1 poise) also matches with this solvent (0.95 poise at 25°C) as well accounting for viscosity effects [69]. Table 4 gives the transferred amount of charge, the charge-transfer distance and the dipole moment induced by the charge transfer calculated from the electronic density difference of **3t** in gas phase, in the presence of implicit solvents of different polarity. All three charge-transfer characteristics increase with solvent polarity. While the

amount of transferred charge increases only slightly with respect to the gas phase with 4.1% for ethylene glycol and 5.2% for water, both the charge-transfer distance (increasing by 14.2% for ethylene glycol and 15.2% for water) and the resulting charge-transfer dipole (18.8% increase for ethylene glycol and 21.2% for water) are significantly influenced by the solvent. Although the dielectric constant of water ($\epsilon_{20^\circ\text{C}}(\text{H}_2\text{O}) = 78.4$) is nearly twice as large as that of ethylene glycol ($\epsilon_{20^\circ\text{C}}(\text{ethylene glycol}) = 37.7$)^[58], the charge transfer characteristics only increase slightly for water compared to ethylene glycol. Previous experiments, including the measurement of absorption and fluorescence spectra, have been carried out using ethylene glycol as a solvent, as some of the combretastatins do not dissolve easily in water. Our results indicate that the charge-transfer properties of combretastatins in aqueous media mimic well experiments using solvents of lower polarity, such as ethylene glycol.

5. Natural charges and WBOs

A detailed analysis of the charge distribution on individual atoms and bonds was undertaken using the Natural Bond Order (NBO) method. The WBOs for the ground and S_1 state of compounds **1-4** for the bonds A, B and C, including the natural charges of representative carbon atoms (where the label C_A corresponds to the aryl carbon of bond A and C_{BA} to the carbon connecting bonds A and B, and vice versa for C_{BC} and C_C) are given in Table 5 (for full data see Supporting Information Table S8 and S9). The WBO values increase with electron density, while the natural charges are lower where the electron density is high. Additionally, the total charge of phenyl ring **I**, its substituents and the $C_{BA}H$ moiety are given, as a measure of the net charge separation in each molecule. Figure 6 shows the overall charge-transfer caused by the $S_0 \rightarrow S_1$ excitation according to the NBO analysis. Areas of electron density depletion are shown in red while areas of electron accumulation are in light blue. The size of the atoms and the thickness of the bonding lines correspond to the magnitude of the change.

The level of charge transfer obtained from the total electron density and the charge separation between two fragments cut at bond B give similar results in all molecules in their ground state, and only increases upon excitation in the case of the charge-transfer derivatives **3** and **4**. The effect of a larger charge separation in the *cis* isomers compared to their *trans* analogues is also confirmed. As previously described, the C=C bond B loses double bond character upon excitation and the WBOs decrease from around 1.8 to around 1.4 for all compounds. However,

the results indicate that the double bond character is slightly less well pronounced for the non-charge transfer compounds, confirming that the latter isomerise more readily than their charge-transfer counterparts. The same cannot be seen when comparing the *trans* isomers with the *cis* isomers: the WBOs of bond B in the S_1 state of the *trans* isomers range from 1.35 to 1.39, while in the *cis* isomers they are markedly higher ($WBO_{S_1/cis}(B) = 1.42 - 1.47$). This suggests that the barrier height is higher for the *cis*→*trans* isomerisation, although our calculated energies for these barriers from the scan show that these energetic barriers are lower when isomerising from the *cis* side with respect to the *trans*→*cis* isomerisation. However, an additional effect driving the *cis*→*trans* isomerisation should be taken into account, namely the steric repulsion between the phenyl rings and the substituents that are spatially close in the *cis* isomers, but at maximum distance from each other in the *trans* configuration.

A closer look at the visualised S_0 → S_1 charge transfer in Figure 6 reveals that, after the excitation, the charge on C_{BA} and C_{BC} for the non-charge transfer compounds **1** and **2** increases (blue spheres) while C_A and C_C donate small amounts of electron density (red spheres). **1** and **2** have electron donating substituents located on the phenyl rings, and it is therefore possible that a non-charge transfer compound with electron pulling substituents on both rings leads to an additional weakening of bond B, which might facilitate the rotation around bond B on the S_1 surface and therefore promote the isomerisation. For the charge transfer analogues **3** and **4**, on the other hand, apart from the afore mentioned larger extent of transferred charge, the charge donation pattern is fundamentally different: the major depletion of charge upon excitation does not only occur for C_A (from the electron donating side), but also from C_{BC} , the atom that links the central C=C bond to the electron pulling phenyl ring **II** (red spheres). The observed localisation of the molecular orbitals contributing to the electron density along bond B towards atom C_{BA} is thus not only an effect of the overall shifted charge along the molecular axis, with a resulting irregular distribution of electron density, but also of an actual depletion of charge at C_{BC} . Interestingly, this does not affect the formal bond orders of bonds A, B and C, which, in the ground state, are similar for the *trans* (1.76-1.79) and *cis* (1.84-1.85) compounds and change after excitation (1.35-1.39 for the *trans* and 1.42-1.47 for the *cis* isomers).

We also carried out an NBO analysis for the S_0 and S_1 states of compounds **1** and **3**, corresponding to values of the scanning coordinate between 180 and -90° . WBO data is not given

for -90° , as the (formerly) π bonding and π^* anti-bonding orbitals of bond B cannot be distinguished. The charge transfer is shown in Figure 7 and all the numerical data is collected in the Supporting Information Tables S10 to S13. The extent of the charge redistribution after excitation decreases monotonically as θ_B approaches the conical intersection with the π/π^* degeneracy. The WBOs, on the other hand, change for both S_0 (from $\text{WBO}_{\text{B}(180^\circ)}(S_0) = 1.68$ to $\text{WBO}_{\text{B}(-100^\circ)}(S_0) = 1.48$ for **1** and from $\text{WBO}_{\text{B}(180^\circ)}(S_0) = 1.67$ to $\text{WBO}_{\text{B}(-100^\circ)}(S_0) = 1.46$ for **3**) and S_1 (from $\text{WBO}_{\text{B}(180^\circ)}(S_1) = 1.26$ to $\text{WBO}_{\text{B}(-100^\circ)}(S_1) = 1.13$ for **1** and from $\text{WBO}_{\text{B}(180^\circ)}(S_1) = 1.30$ to $\text{WBO}_{\text{B}(-100^\circ)}(S_1) = 1.14$ for **3**). As the WBOs decrease approximately by the same amount, the overall bond order is not significantly affected. Analysis of the charge separation during the scan reveals that the disappearance of the charge-transfer character in **3** after excitation near the conical intersection is not due to a decrease in the charge separation between the two fragments separated at bond B. While for **1** the difference in charge between the two molecular fragments is close to 0 throughout the scan on both PES, the charge separation in the ground state of **3** increases from 0.079 at $\theta_B = 180^\circ$ to 0.171 at -100° and 0.217 at -90° . The latter value exceeds the charge separation on the S_1 surface (0.203 at -90°). Interestingly, the charge separation on the S_1 surface decreases during the first steps of the scan until $\theta_B = -130^\circ$, which corresponds to the barrier maximum, and then rises again moving towards the conical intersection, with the smallest charge separation (0.019) at -90° along the C=C rotation coordinate. At this point we also observe a change of trend for the charges of C_{BA} and C_{BC} of bond B in the S_1 state: the charge on C_{BA} (-0.202) exceeds the respective value on C_{BC} (-0.190) up to $\theta_B = -130^\circ$, after which a charge reversal is observed. As these charge effects are not observed in compound **1**, but the bond orders do not significantly differ between compounds **1** and **3**, it seems that the introduction of a charge transfer by substitution of functional groups at the phenyl rings only has a significant effect on the charge distribution on both the S_0 and the S_1 surface, but does not or just to a minor extent affect the isomerisation barriers.

Summary and Conclusion

We have explored the possibility of using electronic structure calculations to tune stilbene derivatives as potential photoactive anti-cancer drugs through the introduction of an intramolecular charge-transfer character using suitable substituent groups. We have carried out DFT and TDDFT calculations of the *trans* and *cis* isomers and the ground and first excited state PES of combretastatin A4 (which has shown cytotoxic behaviour in its *cis*, but not in its *trans*, form) together with three other stilbene derivatives with different charge-transfer character. The charge transfer in these systems is induced by excitation from the ground state (S_0) to the lowest singlet excited state (S_1). The isomerisation coordinate (the rotation around the central C=C double bond) is essentially the same for all molecules in their ground state, while we observe a redshift in absorption wavelengths and a consequent reduction of the relative energies of the S_1 PES with increasing charge-transfer character. Barrier heights on the S_1 surface suggest that both the *trans*→*cis* isomerisation (which is the step necessary to activate the anti-cancer activity of the drug) and the *cis*→*trans* isomerisation are slightly favoured in non-charge transfer derivatives. For non-charge transfer compounds, the *cis*→*trans* isomerisation barrier can be smaller than that for the *trans*→*cis* isomerisation, which could be problematic if photoexcitation of the *cis* isomer cannot be prevented in physiological conditions. The *cis*→*trans* isomerisation barriers for the charge-transfer compounds are of similar height as for the respective *trans*→*cis* isomerisation, which indicates that an even stronger charge-transfer character could reverse the unfavourable *trans*→*cis*/*cis*→*trans* barrier ratio. We have also confirmed that the charge-transfer character increases with the solvent polarity. Furthermore we have shown that the location of the conical intersection along the double bond rotation coordinate is not affected by the charge-transfer character of the molecule. This suggests that, as for unsubstituted stilbene, the *cis*/*trans* product ratio is not influenced by the presence of charge-transfer substituents. We could not identify the formation of a TICT structure or other stable conformations on the S_1 surface, which indicates the absence of competing pathways to the photoinduced S_1 *trans*→*cis* isomerisation. Also, our analysis of the partial charges on individual atoms at excitation suggests different phenyl ring substitution patterns with electron accepting substituents on both sides of the molecule are likely to facilitate the isomerisation process. Our study has shown that the chemical modification of combretastatins and other stilbene derivatives provides a potentially very important route toward the development of new drugs for local cancer therapy.

Acknowledgement

NH and LB thank the Materials Chemistry Consortium for access to the ARCHER UK National Supercomputing Service funded by EPSRC (EP/L000202), the STFC (Science and Technologies Facilities Council) for access to SCARF – Scientific Computing Application Resource for Facilities and the Theoretical Chemistry Group at the University of Marburg for access to the Annemarie cluster for NBO calculations.

Figures and Tables

Table 1: Optimised gas phase and experimental structure data of **1c-4c**. Ground state DFT calculations were carried out at the B3LYP/ def2-TZVPP and CAM-B3LYP/def2-TZVPP levels of theory, and excited-state TDDFT calculations at the CAM-B3LYP/def2-TZVPP one. Distances d are in angstrom and dihedral angles θ in degree. Excited-state structural data is given in italics.

		d_A	d_B	d_C	θ_A	θ_B	θ_C
1c	B3LYP	1.472	1.344	1.470	147.1	-7.0	151.6
	CAM-B3LYP	1.474	1.333	1.472	141.5	-5.8	147.6
	exp	1.470	1.333	1.462	165.3	-9.4	144.0
	<i>CAM-B3LYP</i>	<i>1.401</i>	<i>1.417</i>	<i>1.402</i>	<i>172.4</i>	<i>-44.9</i>	<i>172.6</i>
2c	B3LYP	1.472	1.344	1.469	146.1	-6.9	153.3
	CAM-B3LYP	1.474	1.333	1.471	140.4	-5.7	148.9
	<i>CAM-B3LYP</i>	<i>1.401</i>	<i>1.416</i>	<i>1.401</i>	<i>171.9</i>	<i>-43.8</i>	<i>172.7</i>
	3c	B3LYP	1.472	1.344	1.469	148.3	-7.0
CAM-B3LYP		1.472	1.333	1.471	143.7	-5.7	146.6
<i>CAM-B3LYP</i>		<i>1.404</i>	<i>1.409</i>	<i>1.400</i>	<i>170.3</i>	<i>-36.6</i>	<i>168.3</i>
4c		B3LYP	1.465	1.346	1.468	153.1	-8.0
	CAM-B3LYP	1.468	1.335	1.471	148.3	-6.4	144.4
	<i>CAM-B3LYP</i>	<i>1.404</i>	<i>1.408</i>	<i>1.403</i>	<i>171.9</i>	<i>-37.1</i>	<i>167.7</i>

Table 2: CAM-B3LYP/def2-SVP transferred charge and charge-transfer dipole of *trans* and *cis* isomers of **1-4** obtained from the difference between the S_1 and S_0 electron densities.

	<i>trans</i>		<i>cis</i>	
	Transferred charge/[e]	CT dipole/[D]	Transferred charge/[e]	CT dipole/[D]
1	0.380	0.482	0.420	1.033
2	0.380	0.899	0.421	1.058
3	0.459	5.562	0.556	5.689
4	0.469	6.511	0.594	7.195

Table 3: Absorption and fluorescence properties of the S_1 state of **1-4** calculated at the CAM-B3LYP/def2-TZVPP level of theory.

	Absorption			Fluorescence		
	E (eV)	E (nm)	Osc. Str.	E (eV)	E (nm)	Osc. Str.
1t	3.9621	312.92	1.14021	3.3150	374.00	1.13409
2t	3.9328	315.25	1.11043	3.2626	380.01	1.09243
3t	3.8081	325.57	1.19567	3.1932	388.27	1.23157
4t	3.6812	336.80	1.24440	3.1855	389.21	1.25848
1c	4.2049	294.85	0.53501	2.4882	498.28	0.34496
2c	4.1619	297.90	0.47592	2.4888	498.16	0.34132
3c	4.0060	309.49	0.48169	2.5202	491.95	0.31743
4c	3.8052	325.82	0.53336	2.5472	486.74	0.39942

Table 4: Solvent dependence of the transferred charge, charge-transfer distance and charge-transfer dipole calculated for **3t** from the difference between the S_1 and S_0 electron densities at the CAM-B3LYP/def2-SVP level of theory. The solvents are modelled implicitly using the COSMO [56] approach.

	Transferred charge [e]	CT distance [Å]	CT dipole [Debye]
gasphase	0.459	2.523	5.562
hexane	0.465	2.683	5.995
ethyl acetate	0.473	2.827	6.424
2-propanol	0.476	2.872	6.572
ethanol	0.477	2.877	6.591
methanol	0.477	2.881	6.605
ethylene glycol	0.478	2.882	6.610
DMSO	0.478 (4.1%)	2.884 (14.3%)	6.616 (19.0%)
water	0.483 (5.2)	2.906 (15.2)	6.742 (21.2)

Table 5: CAM-B3LYP/def2-TZVPP WBOs of bonds A, B and C and natural charges (in units of electron charge) of C_A , C_{BA} , C_{BC} , C_C and the electron donating fragment of the molecule (phenyl ring **I**, its substituents and the C_{BC} -H moiety) of **1-4** in the S_0 and S_1 state.

	WBO			Natural charge				
	A	B	C	C_A	C_{BA}	C_{BC}	C_C	Charge separation
1t S_0	1.08	1.79	1.08	-0.049	-0.196	-0.185	-0.076	-0.014
S_1	1.23	1.36	1.23	-0.049	-0.211	-0.226	-0.054	-0.018
2t S_0	1.08	1.79	1.08	-0.052	-0.189	-0.191	-0.077	0.000
S_1	1.23	1.35	1.23	-0.039	-0.218	-0.212	-0.067	0.028
3t S_0	1.08	1.78	1.08	-0.059	-0.167	-0.205	-0.045	0.043
S_1	1.22	1.37	1.23	-0.012	-0.226	-0.162	-0.094	0.162
4t S_0	1.09	1.76	1.09	-0.122	-0.158	-0.226	-0.040	0.083
S_1	1.21	1.39	1.22	-0.031	-0.249	-0.157	-0.106	0.211
1c S_0	1.04	1.85	1.05	-0.062	-0.203	-0.193	-0.089	-0.010
S_1	1.18	1.43	1.19	-0.060	-0.228	-0.245	-0.054	-0.023
2c S_0	1.04	1.85	1.05	-0.066	-0.197	-0.199	-0.090	0.000
S_1	1.19	1.42	1.20	-0.050	-0.236	-0.232	-0.070	0.035
3c S_0	1.04	1.85	1.05	-0.071	-0.179	-0.211	-0.057	0.031
S_1	1.18	1.45	1.20	-0.007	-0.255	-0.167	-0.118	0.223
4c S_0	1.06	1.84	1.05	-0.135	-0.171	-0.229	-0.052	0.062
S_1	1.18	1.47	1.18	-0.009	-0.281	-0.140	-0.147	0.301

Scheme 1: Structure of the stilbene derivatives **1c-4c**.

Figure 1: CAM-B3LYP/def2-TZVPP HOMO and LUMO of **3t** (left) and **3c** (right).

Figure 2: S_1 - S_0 electron density differences calculated with CAM-B3LYP/def2-SVP. Areas of electron depletion are shown in red and areas of electron accumulation in blue.

Figure 3: Absorption and fluorescence (light colours) of compounds **1c-4c** (left) and **1t-4t** (dotted lines, right) calculated with CAM-B3LYP/def2-TZVPP.

Figure 4: S_0 and S_1 PES along the rotational coordinate of bond B with the ground state of the *cis* structures **1c-4c** as reference points. See text for details. Ground and excited state optimised structures are shown as rectangles and their energies from vertical excitation/de-excitation as circles.

Figure 5: Scan of the rotation around bond A (left) and bond C (right) on the S_0 and S_1 PES with the *trans* structures as references. See text for details.

Figure 6: Increase (blue) and decrease (red) in electron density after the $S_0 \rightarrow S_1$ excitation as obtained from WBO and natural charges from NBO calculations with CAM-B3LYP/def2-TZVPP.

Figure 7: Increase (blue) and decrease (red) in electron density after the $S_0 \rightarrow S_1$ excitation as obtained from WBOs and natural charges from NBO calculations with CAM-B3LYP/def2-TZVPP for combretastatin **1** between 180 and -100° (left) and combretastatin **3** between 180 and -100° (right).

References

- [1] Agostinis P, Berg K, Cengel KA, Foster TH, Girotti AW, Gollnick SO, Hahn SM, Hamblin MR, Juzeniene A, Kessel D, Korbelik M, Moan J, Mroz P, Nowis D, Piette J, Wilson BC, Golab J. Photodynamic therapy of cancer: an update. *CA Cancer J Clin.* 2011;61(4):250-281.
- [2] Krukiewicz K, Zak JK. Biomaterial-based regional chemotherapy: Local anticancer drug delivery to enhance chemotherapy and minimize its side-effects. *Mater Sci Eng C Mater Biol Appl.* 2016;62:927-942.
- [3] Pettit GR, Cragg GM, Herald DL, Schmidt JM, Lohavanijaya P. Isolation and structure of combretastatin. *Can J Chem.* 1982;60(11):1374-1376.
- [4] Tron GC, Pirali T, Sorba G, Pagliai F, Busacca S, Genazzani AA. Medicinal chemistry of combretastatin A4: present and future directions. *J Med Chem.* 2006;49(11): 3033-3044.
- [5] Rustin GJS, Galbraith SM, Anderson H, Stratford M, Folkes LK, Sena L, Gumbrell L, Price PM. Phase I clinical trial of weekly combretastatin A4 phosphate: clinical and pharmacokinetic results. *J Clin Oncol.* 2003;21(15):2815-2822.
- [6] Rustin GJ, Shreeves G, Nathan PD, Gaya A, Ganesan TS, Wang D, Boxall J, Poupard L, Chaplin DJ, Stratford MRL, Balkissoon J, Zweifel M. A Phase Ib trial of CA4P (combretastatin A-4 phosphate), carboplatin, and paclitaxel in patients with advanced cancer. *Br J Cancer.* 2010;102(9):1355-1360.
- [7] Scherer KM, Bisby RH, Botchway SW, Parker AW. New Approaches to Photodynamic Therapy from Types I, II and III to Type IV Using One or More Photons. *Anticancer Agents Med Chem.* 2017;17(2):171-189.
- [8] Hepworth LA. New procedures for the photoactivation of anticancer photodrugs [dissertation]. Manchester, UK; University of Manchester Institute of Science and Technology; 2000.
- [9] Lawrence NJ, Rennison D, Woo M, McGown AT, Hadfield JA. Antimitotic and cell growth inhibitory properties of combretastatin A-4-like ethers. *Bioorg Med Chem Lett.* 2001;11(1):51-54.

- [10] Gaukroger K, Hadfield JA, Lawrence NJ, Nolan S, McGown AT. Structural requirements for the interaction of combretastatins with tubulin: how important is the trimethoxy unit? *Org Biomol Chem.* 2003;1(17):3033-3037.
- [11] Lawrence NJ, Hepworth LA, Rennison D, McGown AT, Hadfield JA. Synthesis and anticancer activity of fluorinated analogues of combretastatin A-4. *J Fluor Chemistry.* 2003;123(1):101-108.
- [12] Bisby RH, Botchway SW, Greetham GM, Hadfield JA, McGown AT, Parker AW, Scherer KM, Towrie M. Time-resolved nanosecond fluorescence lifetime imaging and picosecond infrared spectroscopy of combretastatin A-4 in solution and in cellular systems. *Meas Sci Technol.* 2012;23(8):084001.
- [13] Scherer KM, Bisby RH, Botchway SW, Greetham GM, Hadfield JA, Parker AW, Towrie M. Spectroscopy and fluorescence lifetime imaging in live cells of a cyano-substituted combretastatin. *Biomed Spectrosc Imaging.* 2014;3(3):211-218.
- [14] Scherer KM, Bisby RH, Botchway SW, Hadfield JA, Parker AW. Anticancer phototherapy of E-combretastatins by two-photon-induced isomerisation. *J Biomed Opt.* 2015;20(5):051004.
- [15] Scherer KM. Two-photon microscopy of E-combretastatin uptake and activation in live mammalian cells [dissertation]. Salford, UK; University of Salford; 2012.
- [16] Scherer KM, Bisby RH, Botchway SW, Hadfield JA, Haycock JW and Parker AW. Three-dimensional imaging and uptake of the anticancer drug combretastatin in cell spheroids and photoisomerization in gels with multiphoton excitation. *J Biomed Opt.* 2015;20(7):78003-78003.
- [17] Holzmann N, Bernasconi L, Callaghan KM, Bisby RH, Parker AW. Charge transfer in trans-combretastatins. *Chem Phys Lett.* 2018;692:146–151.
- [18] Waldeck DH. Photoisomerization dynamics of stilbenes. *Chem Rev.* 1991;91(3):415-436.
- [19] Takeuchi S, Ruhman S, Tsuneda T, Chiba M, Tetsuya T, Tahara T. Spectroscopic Tracking of Structural Evolution in Ultrafast Stilbene Photoisomerization. *Science.* 2008;322:1073-1077.
- [20] Dietl C, Papastathopoulos E, Niklaus P, Improta R, Santoro F, Gerber G. Femtosecond photoelectron spectroscopy of trans-stilbene above the reaction barrier. *Chem Phys.* 2005;310:201-211.

- [21] Sobolewski AL, Sudholt W, Domcke W. Ab Initio Investigation of Reaction Pathways for Intramolecular Charge Transfer in Dimethylanilino Derivatives. *J Phys Chem A*. 1998;102:2716-2722.
- [22] Parusel ABJ, Köhler G, Grimme S. Density Functional Study of Excited Charge Transfer State Formation in 4-(N,N-Dimethylamino)benzonitrile. *J Phys Chem A*. 1998;102:6297-6306.
- [23] Dreyer J, Kummrow A. Shedding Light on Excited-State Structures by Theoretical Analysis of Femtosecond Transient Infrared Spectra: Intramolecular Charge Transfer in 4-(Dimethylamino)benzonitrile. *J Am Chem Soc*. 2000;120:2577-2585.
- [24] Serrano-Andrés L, Merchán M, Roos BO, Lindh R. Theoretical Study of the Internal Charge Transfer in Aminobenzonitriles. *J Am Chem Soc*. 1995;117:3189-3204.
- [25] Zachariasse KA, von der Haar T, Hebecker A, Leinhos U, Kühnle W. Intramolecular charge transfer in amino-benzonitriles: Requirements for dual fluorescence. *Pure App Chem*. 1993;65(8):1746-1750.
- [26] Nakashima N, Inoue H, Mataga N, Yamanaka C. Time-Resolved Fluorescence Studies on the Dual Fluorescence Process of p-(Dimethylamino)benzonitrile. *Bull Chem Soc Jpn*. 1973;46:2288-2290.
- [27] Hoekstra A. Refinement of the crystal structure of -stilbene (TSB). The molecular structure in the crystalline and gaseous phases. *Acta Crystallogr B*. 1975;31(12):2813-2817.
- [28] Finder CJ. An improved structure of trans-stilbene. *Acta Crystallogr B*. 1974;30(2):411-415.
- [29] Jiang C, Xie R, Li F, Allen RE. Trans-to-cis isomerization of stilbene following an ultrafast laser pulse. *Chem Phys Lett*. 2009;474:263-267.
- [30] Chaudhuri RK, Freed KF, Chattopadhyay S, Mahapatra US. Theoretical Studies of the Ground and Excited State Structures of Stilbene. *J Phys Chem A*. 2013;117:9424-9434.
- [31] Lapouyade R, Czeschka K, Majenz W, Rettig W, Gilabert E, Rulliere C. Photophysics of donor-acceptor substituted stilbenes. A time-resolved fluorescence study using selectively bridged dimethylamino cyano model compounds. *J Phys Chem*. 1992;96(24):9643-9650.

- [32] Pines D, Pines E, Rettig W. Dual fluorescence and excited-state structural relaxations in donor–acceptor stilbenes. *J Phys Chem A*. 2003;107(2):236-242.
- [33] Amatatsu Y. Ab initio study on the photochemical behavior of 4-dimethylamino, 4'-cyanostilbene. *Chem Phys*. 2001;274(2):87-98.
- [34] Yang JS, Liao KL, Hwang CY, Wang CM. Photoinduced single-versus double-bond torsion in donor– acceptor– substituted trans-stilbenes. *J Phys Chem A*. 2006;110(26):8003-8010.
- [35] Yang JS, Lin CK, Lahoti AM, Tseng CK, Liu YH, Lee GH, Peng SM. Effect of ground-state twisting on the trans→ cis photoisomerization and TICT state formation of aminostilbenes. *J Phys Chem A*. 2009;113(17):4868-4877.
- [36] Yang JS, Che-Jen L. Fate of photoexcited trans-aminostilbenes. *J Photochem Photobiol A Chem*. 2015;312:107-120.
- [37] Yao HH, Cheng HH, Cheng CH, Lin CK, Yang JS, Chen IC. Charge-transfer and isomerization reactions of trans-4-(N-arylamino) stilbenes. *Phys Chem Chem Phys*. 2016;18(40):28164-28174.
- [38] Gruen H, Görner H. Fluorescence of Trans-4-Cyano-4'-dimethylaminostilbene; No Evidence for a TICT State. *Z Naturforschung A*. 1983;38(8):928-936.
- [39] Rettig W, Majenz W. Competing adiabatic photoreaction channels in stilbene derivatives. *Chem Phys Lett*. 1989;154(4):335-341.
- [40] Daum R, Hansson T, Nörenberg R, Schwarzer D, Schroeder J. Spectroscopy and dynamics of jet-cooled 4-dimethylamino-4'-cyanostilbene in the S1 state. *Chem Phys Lett*. 1995;246(6):607-614.
- [41] Kovalenko SA, Schanz R, Senyushkina TA, Ernsting NP. Femtosecond spectroscopy of p-dimethylaminocyanostilbene in solution—no evidence for dual fluorescence. *Phys Chem Chem Phys*. 2002;4(5):703-707.
- [42] Farztdinov VM, Ernsting NP. Solvent dependence of structure and electronic properties in the ground and first excited singlet state of 4-dimethylamino-4'-nitrostilbene (DANS)—semiempirical calculations. *Chem Phys*. 2002;277(3):257-270.

- [43] Valiev M, Bylaska EJ, Govind N, Kowalski K, Straatsma TP, Van Dam HHJ, Wang D, Nieplocha J, Apra E, Windus TL, de Jong WA. NWChem: a comprehensive and scalable open-source solution for large scale molecular simulations. *Comput Phys Commun.* 2010;181(9):1477-1489.
- [44] Becke AD. Density-functional thermochemistry. III. The role of exact exchange. *J Chem Phys.* 1993;98(7):5648-5652.
- [45] Lee C, Yang W, Parr RG. Development of the Colle-Salvetti correlation-energy formula into a functional of the electron density. *Phys Rev B.* 1988;37(2):785.
- [46] Weigend F, Ahlrichs R. Balanced basis sets of split valence, triple zeta valence and quadruple zeta valence quality for H to Rn: design and assessment of accuracy. *Phys Chem Chem Phys.* 2005;7(18): 3297-3305.
- [47] Dreuw A, Head-Gordon M. Single-reference ab initio methods for the calculation of excited states of large molecules. *Chem Rev.* 2005;105(11):4009-4037.
- [48] Yanai T, Tew DP, Handy NC. A new hybrid exchange--correlation functional using the Coulomb-attenuating method (CAM-B3LYP). *Chem Phys Lett.* 2004;393(1):51-57.
- [49] Charaf-Eddin A, Planchat A, Mennucci B, Adamo C, Jacquemin D. Choosing a Functional for Computing Absorption and Fluorescence Band Shapes with TD-DFT. *J Chem Theory Comput.* 2013;9:2749-2760.
- [50] Pastore M, Mosconi E, De Angelis F, Grätzel M. A Computational Investigation of Organic Dyes for Dye-Sensitized Solar Cells: Benchmark, Strategies, and Open Issues. *J Phys Chem C.* 2010;114:7205–7212.
- [51] Le Bahers T, Adamo C, Ciofini I. A qualitative index of spatial extent in charge-transfer excitations. *J Chem Theory Comput.* 2011;7(8):2498-2506.
- [52] Jacquemin D, Le Bahers T, Adamo C, Ciofini I. What is the “best” atomic charge model to describe through-space charge-transfer excitations? *Phys Chem Chem Phys.* 2012;14(16):5383-5388.
- [53] Frisch MJ, Trucks GW, Schlegel HB, Scuseria GE, Robb MA, Cheeseman JR, Scalmani G, Barone V, Petersson GA, Nakatsuji H, Li X, Caricato M, Marenich A, Bloino J, Janesko BG,

Gomperts R, Mennucci B, Hratchian HP, Ortiz JV, Izmaylov AF, Sonnenberg JL, Williams-Young D, Ding F, Lipparini F, Egidi F, Goings J, Peng B, Petrone A, Henderson T, Ranasinghe D, Zakrzewski VG, Gao J, Rega N, Zheng G, Liang W, Hada M, Ehara M, Toyota K, Fukuda R, Hasegawa J, Ishida M, Nakajima T, Honda Y, Kitao O, Nakai H, Vreven T, Throssell K, Montgomery Jr. JA, Peralta JE, Ogliaro F, Bearpark M, Heyd JJ, Brothers E, Kudin KN, Staroverov VN, Keith T, Kobayashi R, Normand J, Raghavachari K, Rendell A, Burant JC, Iyengar SS, Tomasi J, Cossi M, Millam JM, Klene M, Adamo C, Cammi R, Ochterski JW, Martin RL, Morokuma K, Farkas O, Foresman JB, Fox DJ. Gaussian 09, Revision A.02. Gaussian, Inc.; Wallingford CT; 2016.

[54] Wiberg K. Application of the pople-santry-segal CNDO method to the cyclopropylcarbinyll and cyclobutyl cation and to bicyclobutane. *Tetrahedron*. 1968;24(3):1083-1096.

[55] Weinhold F, Landis C. Valency and Bonding, A Natural Bond Orbital Donor –Acceptor Perspective. Cambridge, UK. Cambridge University Press; 2005.

[56] Klamt A, Schurmann GJ. COSMO: a new approach to dielectric screening in solvents with explicit expressions for the screening energy and its gradient. *J Chem Soc Perkin 1*. 1993;2(5):799–805.

[57] York DM, Karplus M. A smooth solvation potential based on the conductor-like screening model. *J Phys Chem A*. 1999;103(50):11060–11079.

[58] Lide DR. CRC Handbook of Chemistry and Physics 2004-2005: A Ready-Reference Book of Chemical and Physical Data. CRC Press; 2006.

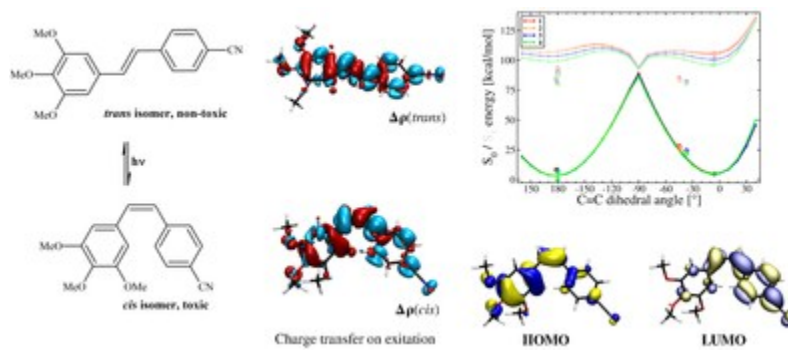
[59] Lara-Ochoa F, Espinosa-Perez G. A new synthesis of combretastatins A-4 and AVE-8062A. *Tetrahedron Lett*. 2007;48(39):7007-7010.

[60] Kwasniewski SP, Claes L, François JP, Deleuze MS. High level theoretical study of the structure and rotational barriers of trans-stilbene. *J Chem Phys*. 2003;118(17):7823-7836.

[61] Choi CH, Kertesz M. Conformational information from vibrational spectra of styrene, trans-stilbene, and cis-stilbene. *J Phys Chem A*. 1997;101(20):3823-3831.

[62] Impropa R, Santoro F. Excited-state behavior of trans and cis isomers of stilbene and stiff stilbene: A TD-DFT study. *J Phys Chem A*. 2005;109(44):10058-10067.

-
- [63] Fabrizio A, Corminboeuf C. How do London Dispersion Interactions Impact the Photochemical Processes of Molecular Switches? *J Phys Chem Lett.* 2018;9(3):464-470.
- [64] Hilborn RC. Einstein coefficients, cross sections, f values, dipole moments, and all that. *Am J Phys.* 1982;50(11):982-994.
- [65] Levine BG, Ko C, Quenneville J, Martínez TJ. Conical intersections and double excitations in time-dependent density functional theory. *Mol Phys.* 2006;104(5-7):1039-1051.
- [66] Zhang X, Herbert JM. Analytic derivative couplings for spin-flip configuration interaction singles and spin-flip time-dependent density functional theory. *J Chem Phys.* 2014;141(6):064104.
- [67] Quenneville J, Martinez TJ. Ab initio study of cis– trans photoisomerization in stilbene and ethylene. *J Phys Chem A.* 2003;107(6):829-837.
- [68] Ben-Nun M, Martínez TJ. Photodynamics of ethylene: Ab initio studies of conical intersections. *Chem Phys.* 2000;259(2-3):237-248.
- [69] Bisby RH, Botchway SW, Hadfield JA, McGown AT, Parker AW, Scherer KM. Fluorescence lifetime imaging of E-combretastatin uptake and distribution in live mammalian cells. *Eur J Cancer.* 2012;48(12):1896-1903.



33x14mm (300 x 300 DPI)